JSC-14694

Shuttle Entry Guidance

Mission Planning and Analysis Division

February 1979

National Aeronautics and
Space Administration

Lyndon B. Johnson Space Center
Houston, Texas

79-FM-7

JSC-14694

SHUTTLE PROGRAM

SHUTTLE ENTRY GUIDANCE

By Jon C. Harpold and Claude A. Graves
Flight Analysis Branch

Approved: Claude A. Graves, Jr.
Claude A. Graves, Assistant Chief
Flight Analysis Branch

Approved: Ronald L. Berry
Ronald L. Berry, Chief
Mission Planning and Analysis Division

Mission Planning and Analysis Division

National Aeronautics and Space Administration

Lyndon B. Johnson Space Center

Houston, Texas

February 1979

CONTENTS

TABLES

FIGURES

SHUTTLE ENTRY GUIDANCE

Jon C. Harpold
Claude A. Graves, Jr.

This paper describes the design of the entry guidance for the Space Shuttle Orbiter. This guidance provides the steering commands for trajectory control from initial penetration of the Earth's atmosphere until the terminal area guidance is activated at an Earth-relative speed of 2500 fps. At this point, the Orbiter is at a distance of about 50 nmi from the runway threshold, and at an altitude of about 80 000 ft. The entry guidance design is based on an analytic solution of the equations of motion defining the drag acceleration profile that meets the terminal criteria of the entry flight while maintaining the flight within systems and operational constraints. Guidance commands, which are based on a control law that ensures damping of oscillatory type trajectory motion, are computed to steer the Orbiter to this drag acceleration profile.

INTRODUCTION

The entry guidance for the Space Shuttle Orbiter provides steering commands to control the entry trajectory from initial penetration of the Earth's atmosphere (altitude of 400 000 ft and range of approximately 4100 nmi from runway) until activation of the terminal area guidance at an Earth-relative speed of 2500 fps. At the latter point, the Orbiter is approximately 50 nmi from the runway threshold at an altitude of about 80 000 ft. The primary objectives of the entry guidance are (1)

to guide the Orbiter along a path that minimizes the demands on the Orbiter systems design throughout the Orbiter missions and (2) to deliver the Orbiter to a satisfactory energy state and vehicle attitude at the initiation of the terminal area guidance system.

The mission spectrum over which the guidance must operate includes missions with orbit inclinations varying from 28.5 degrees to 104 degrees, orbit altitudes up to 500 nmi and Orbiter weights between 150 000 lb and 227 000 lb with the longitudinal center of gravity varying between 65 percent and 67.5 percent of the Orbiter length. For each of these operational flights, the entry guidance must also have the flexibility to provide sufficient return opportunities from orbit as well as the capability for return to Earth at the end of the first orbit in the event an abort is required during the ascent-powered flight. In addition, the guidance must be able to adapt to changes in systems constraints as the Orbiter design evolves and to permit optimization of the profile shape to minimize demands on the Orbiter systems performance for the initial test flight program that must be flown before the Orbiter systems performance is well established.

The Orbiter systems that are of most concern during entry are the thermal protection system (TPS), the flight control system (FCS), and the Orbiter structure. The TPS is a reusable system consisting of several components that limit the allowable surface temperature of the Orbiter. The heat load into the structure must be minimized to achieve minimum thickness and weight of the TPS required for insulation of the Orbiter structure. Entry flight analysis has demonstrated that the minimum insulation weight is achieved by flying the maximum angle of attack consistent with the crossrange requirement. For the Space Shuttle operational flights, this is achieved by maintaining an angle of attack of 38 degrees during the period of high heating rate and then reducing this angle of attack to about 28 degrees to achieve good crossranging characteristics. The early flight tests have low orbit inclinations, and hence relatively low crossrange requirements. Thus, the angle-of-attack profile for these flights does not require reducing the angle of attack for crossrange purposes; therefore, a 40-degree angle-of-attack

profile can be maintained for an extended period on these initial flights to provide additional TPS performance margins.

The vehicle attitude maneuvering demanded by the guidance is minimized to provide a smooth flight and lessen the demands on the flight control system. Because a combination of aerodynamic control surface movement and reaction control system (RCS) thrusters are used for attitude control during entry, minimizing the attitude maneuvering demands will minimize the RCS propellant requirement and the propellant required by the auxiliary propulsion unit that provides the energy to move the aerodynamic control surfaces. To limit demands on the FCS, the bank angle angular acceleration and rate are limited to 1.7 deg/sec^2 and 5 deg/sec, respectively, and the pitch acceleration and rate are limited to 5 deg/sec^2 and 2 deg/sec, respectively. The entry trajectory is further constrained to limit the dynamic pressure so that aerodynamic control surface hinge moments are small and to limit the flight regime where the FCS is required to meet lateral directional stability requirements.

To minimize the Orbiter internal structure weight, the aerodynamic loads are limited during entry. Because the total aerodynamic force during entry is essentially perpendicular to the Orbiter longitudinal axis, this is achieved by limiting the normal aerodynamic load factor to 2.5 g's.

The flight constraints discussed up to this point limit the minimum Orbiter altitude at any given velocity during entry. The maximum altitude is limited by the ability of the Orbiter to maintain equilibrium flight conditions; i.e., the capability of the Orbiter to maintain the present flightpath angle rate.

Because the terminal area guidance requires flight on the front side of the vehicle lift-to-drag (L/D) curve, the entry guidance must deliver the Orbiter to this point with an angle of attack no greater than the value corresponding to maximum L/D. This is achieved by a pitchdown maneuver, beginning at an Earth-relative speed of approximately 14 000 fps, designed to reduce the angle of attack from the high value during

the early part of the entry flight to a value near maximum L/D at an Earth-relative speed of 2500 fps. Typical angle-of-attack profiles during entry for the operational flights and for the early flight tests are illustrated in Fig. 1. The entry flight corridor as constrained by the

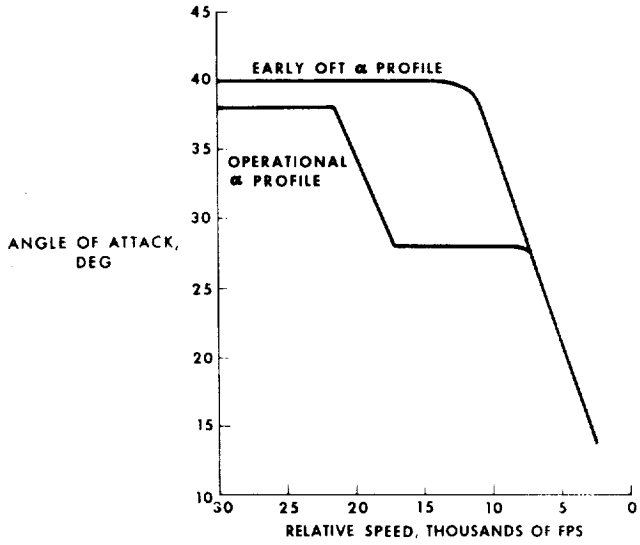

Figure 1.- Angle-of-attack profiles for the OFT and operational flights.

TPS surface temperatures, normal load factor, dynamic pressure, and equilibrium glide flight limits can be uniquely defined in the drag acceleration Earth-relative velocity plane. Typical corridors for the operational and flight test angle-of-attack profiles are illustrated in Fig. 2. The heat load accumulated from the aerodynamic heating during entry is not unique in this plane. However, a general trend of decreasing heat load, as the altitude is reduced and hence drag acceleration is increased, is well established. Thus, the structure temperature behind the insulation of the TPS is decreased as the drag acceleration increases.

GUIDANCE CONCEPT

The range to be flown during entry is a unique function of the drag acceleration profile maintained throughout the entry flight. This entry range is predictable using analytic techniques for simple geometric drag acceleration functions of Earth-relative speed, provided the local

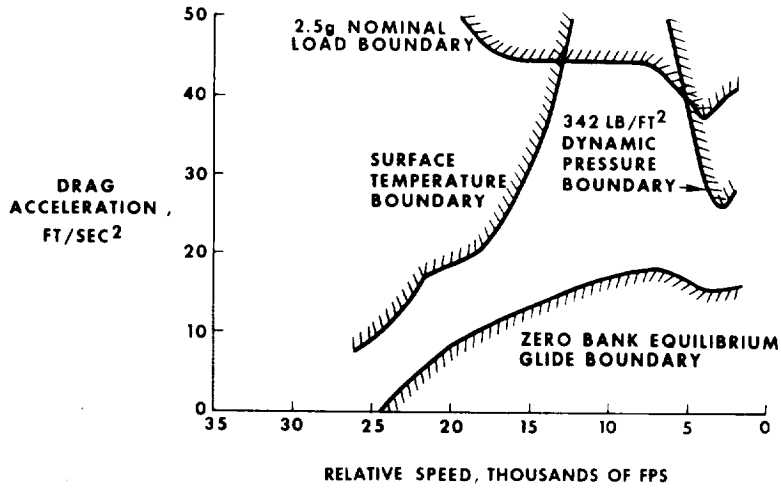

(a) Operational angle-of-attack profile.

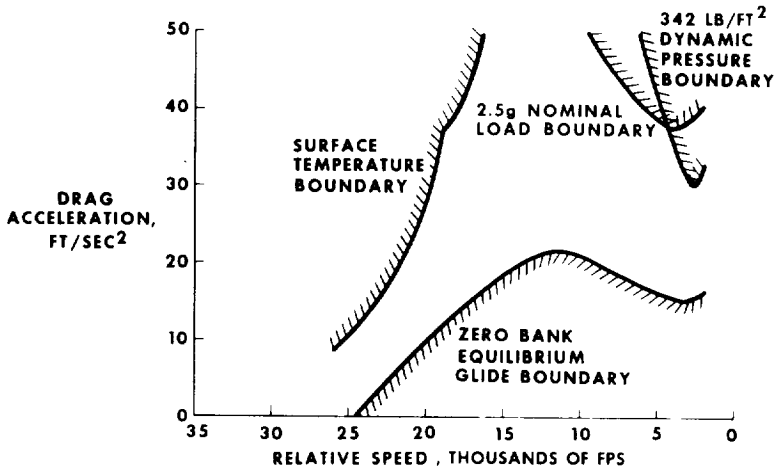

(b) Flight test program angle-of-attack profile.

Figure 2.- Flight corridor.

flightpath angle is near zero. For low speeds where the flightpath angle is not sufficiently near zero, range predictions can be analytically computed for simple geometric drag acceleration functions if the independent variable is changed from Earth-relative speed to energy with respect to the Earth. Flight throughout the entry corridor can be achieved by linking these geometric functions together in a series. The Space Shuttle Orbiter entry guidance is designed on the principle of analytically defining a desired drag acceleration profile and commanding the Orbiter attitudes to achieve the desired profile.

This drag acceleration profile shape is designed by input constants to have a form that best fits within the entry corridor and that also minimizes the accumulated aerodynamic heat load. Prediction of the entry range that will be flown along this profile from the present state during entry to the termination of the entry flight phase is predicted using analytical solutions to the equations of motion. The level of the drag acceleration profile is adjusted, while retaining the basic profile shape, such that the predicted range and the range to the target are the same value. The drag acceleration profile is defined as the reference drag acceleration profile. The altitude rate and the component of L/D in the plane formed by the position and Earth-relative velocity vectors, which correspond to this drag acceleration profile, can also be computed analytically.

With the definition of the desired entry profile, a control law was developed to compute guidance commands to control the Orbiter to this profile. This control law was developed using linearized analysis of the flight dynamics. The resultant control law response to disturbance from the reference profile is represented by a homogenous second-order differential equation with constant coefficients. The transient response characteristics of this differential equation are well understood, thus development of the gains for the feedback terms of the control law to provide the desired transient response is a simple matter. The control law resulting from this analysis is as follows:

$$(L/D)_c = (L/D)_0 + f_1 (D - D_0) + f_2 (\dot{h} - \dot{h}_0) + f_4 \int (D - D_0) \qquad (1)$$

The last term of this control law prevents steady-state trajectory deviations because of inaccuracy in determining altitude rate by the navigation system.

The commanded L/D, which is the component of L/D in the plane formed by the position and Earth-related velocity vectors, can be achieved by angle-of-attack modulation, by bank angle modulation, or by a combination of the two. The Orbiter entry guidance uses a combination of bank

angle and angle-of-attack modulation for trajectory control. Bank angle was chosen as the primary trajectory control parameter because the angle of attack can then be selected to minimize the aerodynamic heating environment while achieving the required crossrange. This also minimizes changes in the aerodynamic heating distribution over the Orbiter because of changes in the angle of attack. Therefore, bank angle is used to control both the total entry range and the crossrange component of entry range. The magnitude of the bank angle controls total range, and the direction of the bank angle controls the Orbiter heading relative to the path required to initiate the turn onto the runway final approach. When the Orbiter heading relative to the desired path exceeds a predetermined value, the bank angle direction is reversed to reduce the heading deviation.

Because the trajectory response to bank angle modulation is relatively slow, particularly with the low bank angle acceleration and rate capability, the angle of attack is modulated to achieve the reference drag acceleration on a short period basis. The bank angle is modulated to control the angle of attack to the reference profile on a long period basis. This capability is designed primarily to reduce the excursions from the nominal dynamic pressure profile caused by large crosswinds at speeds below 10 000 fps. This feature also reduces the phugoid motion induced when the bank angle direction is reversed to control the Orbiter heading and provides additional maneuverability to compensate for trajectory dispersions.

THEORETICAL ANALYSIS

This section presents the development of closed form solutions to the equations of motion that predict the range flown with different geometric drag acceleration profile shapes as well as for computing reference trajectory parameters along these profiles. In addition, a control law is developed that provides steering commands to achieve good transient response in controlling the Orbiter to the drag acceleration profile that is selected to achieve specified entry terminal conditions while maintaining the profile within the entry corridor.

Examination of the entry corridor presented in Fig. 2 shows that an entry profile consisting of pseudoequilibrium glide, quadratic, linear, and constant drag acceleration profile segments as a function of Earth-relative speed can be linked together to provide the capability to achieve essentially any desired profile within the entry corridor. Therefore, the guidance equations are developed for these profiles.

The equations of motion used in this analysis are developed in a coordinate system with one axis oriented along the Earth-relative velocity vector, one axis perpendicular to the plane formed by the position and Earth-relative velocity vectors, and the third axis completing the right-hand coordinate system. These equations of motion are as follows:

$$\dot{V} = D - g \sin \gamma \tag{2}$$

$$V\dot{\gamma} = \left(\frac{V^2}{r} - g\right) \cos \gamma + L_V \cos \phi \tag{3}$$

$$V \cos \gamma \dot{\psi} = \frac{V^2}{r} \cos^2 \gamma \sin \psi \tan \theta + L_V \sin \phi \tag{4}$$

These equations of motion neglect the Coriolis and centripetal accelerations due to the Earth's rotation because these accelerations are small compared to the aerodynamic acceleration.

Range Prediction

The time rate of change of range is given by

$$\dot{R} = V \cos \gamma \tag{5}$$

The predicted range is determined by integrating the following equation that results from combining Eqs. (2) and (5).

$$R = -\int \frac{V \cos \gamma \, dV}{D + g \sin \gamma} \tag{6}$$

For the small flightpath angles that occur for the early part of entry where the Orbiter is at high speed, this equation can be reduced to the following equation by assuming $\cos \gamma = 1$ and $\sin \gamma = 0$.

$$R = -\int \frac{V dV}{D} \tag{7}$$

The drag acceleration is expressed as simple functions of Earth-relative speed, and then the integration to obtain closed form range prediction equations is straightforward. The resulting range predictions are defined for pseudoequilibrium glide, quadratic, linear, and constant drag acceleration function of Earth-relative speed in Table 1. Equilibrium glide/flight occurs when the flightpath angle is constant. Therefore, the drag acceleration for this condition, assuming $\cos \gamma = 1$, is determined from Eq. (3).

$$D = \frac{\left(g - \frac{V^2}{r}\right)}{L/D} \tag{8}$$

To provide more flexibility in shaping the entry profile, the pseudoequilibrium glide equation introduces an arbitrary constant as follows:

$$D = \frac{g}{\left(\frac{L}{D}\right)} \left[1 - \frac{V^2}{VS^2}\right] \quad \text{where } VS^2 = \text{arbitrary constant} \tag{9}$$

During the latter part of entry when the Orbiter is at a low speed, the flightpath angle, γ, becomes more negative. In this case, a change of the independent variable from Earth-relative speed to energy with respect to the Earth results in a more accurate expression for entry range. The expression for range is obtained as follows:

$$E = gh + 1/2V^2 \tag{10}$$

This equation is differentiated with respect to altitude to obtain

$$\frac{dE}{dH} = g + V\frac{dV}{dh} \tag{11}$$

The derivative $\frac{dV}{dH}$ is obtained by noting that

$$\dot{h} = V \sin \gamma \tag{12}$$

and combining this equation with Eq. (2) to obtain the following results:

$$\frac{dV}{dh} = \frac{-D}{V \sin \gamma} - \frac{g}{V} \tag{13}$$

Eq. (13) is then combined with Eq. (11) to obtain the following equation:

$$\frac{dE}{dh} = \frac{-D}{\sin \gamma} \tag{14}$$

From geometry

$$\frac{dh}{dR} = \tan \gamma \tag{15}$$

Eqs. (14) and (15) are combined to obtain the following expression for range:

$$R = \int \frac{-\cos \gamma \, dE}{D} \tag{16}$$

Even for a relatively large magnitude of flightpath angle $\cos \gamma = 1$; therefore, this equation becomes

$$R = -\int \frac{dE}{D} \tag{17}$$

The predicted range can be determined by integrating Eq. (17) for simple drag acceleration functions of energy. When the magnitude of flightpath angle is such that $\sin \gamma$ is not sufficiently near zero, this results in more accurate range predictions than integrating Eq. (7). The range

equation for a linear drag acceleration function of energy is presented in Table 1.

TABLE 1.- ENTRY RANGE PREDICTIONS

Phase	Drag Segment Form	Range Prediction Equation
Temperature Control	$D = C_1 + C_2V + C_3V^2$	$Q = 4C_3C_1 - C_2^2$ If $Q > 0$ $R_1 = \frac{-1}{2C_3} \text{LOG} \left[\frac{C_1 + C_2V_F + C_3V_F^2}{C_1 + C_2V + C_3V^2} \right] + \frac{C_2}{C_3\sqrt{Q}} \left[\text{TAN}^{-1} \left[\frac{2C_3V_F + C_2}{\sqrt{Q}} \right] - \text{TAN}^{-1} \left[\frac{2C_3V + C_2}{\sqrt{Q}} \right] \right]$ If $Q < 0$ $R_1 = \frac{-1}{2C_3} \text{LOG} \left[\frac{C_1 + C_2V_F + C_3V_F^2}{C_1 + C_2V + C_3V^2} \right] + \frac{C_2}{2C_3\sqrt{-Q}} \text{LOG} \left[\frac{2C_3V_F + C_2 - \sqrt{-Q}}{2C_3V_F + C_2 + \sqrt{-Q}} \frac{2C_3V + C_2 - \sqrt{-Q}}{2C_3V + C_2 + \sqrt{-Q}} \right]$
Equilibrium Glide	$D = \frac{g}{\frac{L}{D}} \left[1 - \frac{V^2}{V_S^2} \right]$	$R_2 = 0.5 \left[\left[\frac{V_S^2 - V^2}{D} \right] \text{LOG} \left[\frac{V_F^2 - V_S^2}{V^2 - V_S^2} \right] \right]$
Constant Drag	$D = C_4$	$R_3 = \frac{V^2 - V_F^2}{2C_4}$
Transition	$D = D_F + C_5 (E - E_F)$	$R_4 = \frac{(E - E_F)}{(D - D_F)} \text{LOG} \left[\frac{D}{D_F} \right]$

Reference Trajectory Parameters

The formulation of equations to determine the L/D and altitude rate corresponding to the drag acceleration profile (reference trajectory parameters) is developed in this section. These reference trajectory pa-

rameters are used by the control law developed to issue commands to steer the Orbiter to the desired entry profile.

Because the magnitude of the flightpath angle is small, the altitude rate is accurately defined by

$$\dot{h} = V\gamma \tag{18}$$

then

$$\ddot{h} = V\dot{\gamma} + \gamma\dot{V} \tag{19}$$

Combining Eq. (19) with Eqs. (2) and (3) and assuming $\cos\gamma = 1$ and $\gamma^2 = 0$, the following equation results:

$$\ddot{h} = -D\frac{\dot{h}}{V} + \left(\frac{V^2}{r} - g\right) + (L/D)D \tag{20}$$

Assuming an exponential atmosphere of the form

$$\rho = \rho_0 e^{-\frac{h}{hs}} \tag{21}$$

Then,

$$\frac{\dot{\rho}}{\rho} = -\frac{\dot{h}}{hs} \tag{22}$$

Since

$$D = 1/2\ \rho V^2 \frac{C_D S}{m} \tag{23}$$

Then,

$$\frac{\dot{D}}{D} = \frac{\dot{\rho}}{\rho} + \frac{2\dot{V}}{V} + \frac{\dot{C}_D}{C_D} \tag{24}$$

Eq. (24) is combined with Eq. (2), with $\sin\gamma$ assumed to be zero, and with Eq. (22) to define a general expression for altitude rate.

$$\dot{h} = -hs \left[\frac{\dot{D}}{D} + \frac{2D}{V} - \frac{\dot{C}_D}{C_D} \right] \tag{25}$$

Eq. (25) is then differentiated and combined with Eq. (2) to obtain the following expression:

$$\ddot{h} = -hs \left[\frac{2\dot{D}}{V} + \frac{2D^2}{V^2} + \frac{\ddot{D}}{D} - \frac{\dot{D}^2}{D^2} + \frac{\dot{C}_D{}^2}{C_D{}^2} - \frac{\ddot{C}_D}{C_D} \right] \tag{26}$$

Eqs. (20), (25), and (26) are combined to obtain the following differential equation that relates drag acceleration and the derivative of drag acceleration to L/D, C_D, and derivatives of C_D.

$$\ddot{D} - \dot{D}\left(\frac{\dot{D}}{D} - \frac{3D}{V} \right) + \frac{4D^3}{V^2} = -\frac{D}{hs}\left(\frac{V^2}{r} - g \right) - \frac{D^2}{hs} L/D - \frac{\dot{C}_D D}{C_D}\left(\frac{\dot{C}_D}{C_D} - \frac{D}{V} \right) + \frac{\ddot{C}_D D}{C_D} \tag{27}$$

Eqs. (25) and (27) define general expressions for the altitude rate and L/D corresponding to drag acceleration and drag coefficient profiles. The functions for these two parameters can be determined for specific drag acceleration and drag coefficient profiles once these profiles are defined. Because the angle-of-attack profile is selected based on aerodynamic heating and crossrange considerations, the drag coefficient profile is also determined by these considerations. Therefore, at this point, the reference L/D and altitude rate retain generalization for the drag coefficient profile. Note that during entry for a constant angle of attack, the drag coefficient is approximately constant; therefore, the drag coefficient derivatives are very small.

The reference trajectory parameters for a quadratic drag acceleration profile as a function of Earth-relative speed are developed as an exam-

ple. The reference trajectory parameters for the remaining drag acceleration profiles are defined in Table 2.

TABLE 2.- REFERENCE TRAJECTORY PARAMETERS

Phase	D_0	$\dot{h}_0$	$(L/D)_0$
Temperature Control	$C_1 + C_2V + C_3V^2$	$\frac{-hs}{V}\left[2C_1 + C_2V - \frac{\dot{C}_{D_0}V}{C_{D_0}}\right]$	$\frac{g}{D_0}\left(1 - \frac{V^2}{V_S^2}\right) - \frac{4hsC_1}{V^2} - \frac{hsC_2}{V}$ $- \frac{hs\dot{C}_{D_0}}{C_{D_0}D_0}\left(\frac{\dot{C}_{D_0}}{C_{D_0}} - \frac{D_0}{V}\right) + \frac{hs\ddot{C}_{D_0}}{C_{D_0}D_0}$
Equilibrium Glide	$\frac{g}{\frac{L}{D}}\left[1 - \frac{V^2}{V_S^2}\right]$	$\frac{-hs}{V}\left[\frac{2D_0}{\left[1 - \frac{V^2}{V_S^2}\right]} - \frac{\dot{C}_{D_0}V}{C_{D_0}}\right]$	$\frac{g}{D_0}\left(1 - \frac{V^2}{V_S^2}\right) - \frac{4hsD_0}{V^2\left[1 - \frac{V^2}{V_S^2}\right]}$ $- \frac{hs\dot{C}_D}{C_{D_0}D_0}\left(\frac{\dot{C}_{D_0}}{C_{D_0}} - \frac{D_0}{V}\right) + \frac{hs\ddot{C}_{D_0}}{C_{D_0}D_0}$
Constant Drag	C_4	$-hs\left[\frac{2D_0}{V} - \frac{\dot{C}_{D_0}}{C_{D_0}}\right]$	$\frac{g}{D_0}\left(1 - \frac{V^2}{V_S^2}\right) - \frac{4hsD_0}{V^2} - \frac{hs\dot{C}_{D_0}}{C_{D_0}D_0}\left(\frac{\dot{C}_{D_0}}{C_{D_0}} - \frac{D_0}{V}\right)$ $+ \frac{hs\ddot{C}_{D_0}}{C_{D_0}D_0}$
Transition Phase	$D_F + C_5(E - E_F)$	$-hs\left[\frac{2D_0V - C_5V^3}{V^2 + 2hsg} - \frac{\dot{C}_{D_0}V}{C_{D_0}}\right]$	$\frac{g}{D_0}\left(1 - \frac{V^2}{V_S^2}\right)$ $+ \frac{\left[2V\dot{h}_0 + \frac{2\dot{h}_0^2g}{D} - hsC_5V^2 + 2D_0hs + 2g\dot{h}_0\frac{hs}{V} - 3C_5Vg\dot{h}_0\frac{hs}{D_0}\right]}{V^2 + 2ghs}$ $+ \frac{\dot{h}_0}{V} + \frac{g}{D_0}\frac{\dot{h}^2}{V^2} - \frac{hs\dot{C}_{D_0}}{C_{D_0}D_0}\left(\frac{\dot{C}_{D_0}}{C_{D_0}} - \frac{D_0}{V}\right) + \frac{hs\ddot{C}_{D_0}}{C_{D_0}D_0}$

Note: C_1, C_2, C_3, L/D, C_4, and C_5 are selected to produce a total drag profile consistent with the range requirements as produced by the range equations in Table 1.

The drag acceleration profile is defined by

$$D = C_1 + C_2V + C_3V^2 \tag{28}$$

This equation is differentiated and combined with Eq. (2) to obtain

$$\frac{\dot{D}}{D} = -C_2 - 2C_3V \tag{29}$$

This is combined with Eq. (25) to obtain the following expression for reference altitude rate:

$$\dot{h}_0 = -\frac{hs}{V}\left[2C_1 + C_2V - \frac{\dot{C}_{D_0}V}{C_{D_0}}\right] \tag{30}$$

Eq. (29) is differentiated and combined with Eq. (2), assuming sin γ = 0, to obtain the following expression for $\frac{\ddot{D}}{D^2}$

$$\frac{\ddot{D}}{D^2} = \frac{(C_2 + 2C_3V)^2}{D} + 2C_3 \tag{31}$$

Eqs. (27), (28), (29), and (31) are combined to obtain the following expression for the reference L/D.

$$(L/D)_0 = -\frac{1}{D_0}\left(\frac{V^2}{r} - g\right) - \frac{4hsC_1}{V^2} - \frac{hsC_2}{V} - \frac{hs\dot{C}_{D0}}{C_{D_0}D_0}\left(\frac{\dot{C}_{D_0}}{C_{D_0}} - \frac{D_0}{V}\right) + \frac{hs\ddot{C}_{D_0}}{C_{D_0}D_0} \tag{32}$$

Control Law

In practice, deviations from the reference profile will occur because of inaccuracies in modeling the reference trajectory parameters and the environment, navigation inaccuracies, bank reversal required for crossrange trajectory control, and delays in executing the commands through the flight control system. A control law based on linearized analysis of the flight dynamics, which ensures damping of oscillatory type trajectory motion, is developed in this section.

The following linear relationships for small deviations from the reference values are defined:

$$\delta\ddot{D} = \ddot{D} - \ddot{D}_0$$

$$\delta\dot{D} = \dot{D} - \dot{D}_0$$

$$\delta D = D - D_0$$

$$\delta V = V - V_0$$

$$\delta(L/D) = (L/D)_C - (L/D)_0 \tag{33}$$

Using first-order difference equations, Eq. (27) becomes

$$\delta\ddot{D} + \left[\frac{3D_0}{V_0} - \frac{2\dot{D}_0}{D_0}\right]\delta\dot{D} + \left[3\dot{D}_0\left(\frac{\dot{D}_0}{D_0^2} - \frac{1}{V_0}\right) + \frac{4D_0^2}{V_0^2} - \frac{1}{hs}\left(\frac{V_0^2}{r_0} - g\right) - \frac{2\ddot{D}_0}{D_0} - \frac{\dot{C}_{D_0}^2}{C_{D_0}^2} + \frac{\ddot{C}_{D_0}}{C_{D_0}}\right]\delta D$$

$$+ \left[\frac{2D_0V_0}{hsr_0} - \frac{3\dot{D}_0D_0}{V_0^2} - \frac{8D_0^3}{V^3} + \frac{\dot{C}_{D0}D_0^2}{C_{D_0}V_0^2}\right]\delta V = -\frac{D_0^2}{hs}\delta(L/D)$$

$$+ \frac{D_0}{C_{D_0}}\ddot{\delta C}_D + \left[\frac{D_0^2}{C_{D_0}V_0} - \frac{2D_0\dot{C}_{D_0}}{C_{D_0}^2}\right]\dot{\delta C}_D$$

$$+ \left[\frac{2\dot{C}_{D_0}^2 D_0}{C_{D_0}^3} - \frac{\dot{C}_{D_0} D_0^2}{C_{D_0}^2 V_0} - \frac{\ddot{C}_{D_0} D_0}{C_{D_0}^2}\right]\delta C_D \tag{34}$$

The Orbiter uses bank angle modulation for ranging; therefore, δC_D and the derivatives of δC_D are zero.

A linear feedback function of the following form is used to provide a means for achieving desirable dynamic response in controlling the Orbiter to the reference profile.

$$\delta(L/D) = f_1'\delta D + f_2'\dot{\delta D} + f_3'\delta V \tag{35}$$

Then with δC_D and the derivatives of δC_D equal to zero, Eqs. (34) and (35) become

$$\delta\ddot{D} + \left[\frac{D_0^2}{hs}f_2' + \frac{3D_0}{V_0} - \frac{2\dot{D}_0}{D_0}\right]\delta\dot{D} + \left[\frac{D_0^2 f_1'}{hs} + 3\dot{D}_0\left(\frac{\dot{D}_0^2}{D_0^2} - \frac{1}{V_0}\right) + \frac{4D_0^2}{V_0^2}\right.$$

$$\left. - \frac{1}{hs}\left(\frac{V_0^2}{r_0} - g\right) - \frac{2\ddot{D}_0}{D_0} - \frac{\dot{C}_{D_0}^2}{C_{D_0}^2} + \frac{\ddot{C}_{D_0}}{C_{D_0}}\right]\delta D + \left[\frac{D_0^2 f_3'}{hs} + \frac{2D_0V_0}{hsr_0}\right.$$

$$\left. - \frac{3\dot{D}_0D_0}{V_0^2} - \frac{8D_0^3}{V_0^3} + \frac{\dot{C}_{D_0}D_0^2}{C_{D_0}V_0^2}\right]\delta V = 0 \qquad (36)$$

This second order, homogenous equation with constant coefficients is in the form of a damped oscillator defined by

$$\delta\ddot{D} + 2\zeta\omega\delta\dot{D} + \omega^2\delta D = 0 \qquad (37)$$

The feedback terms are expressed in terms of the damping ratio, undamped natural frequency and reference trajectory parameters by combining Eqs. (36) and (37).

$$f_1' = \frac{hs}{D_0^2}\left[\omega^2 + 3\dot{D}_0\left(\frac{1}{V_0} - \frac{\dot{D}_0}{D_0^2}\right) + \frac{1}{hs}\left(\frac{V_0^2}{r_0} - g\right) - \frac{4D_0^2}{V_0^2}\right.$$

$$\left. + \frac{2\ddot{D}_0}{D_0} + \frac{\dot{C}_{D_0}^2}{C_{D_0}^2} + \frac{\ddot{C}_{D_0}}{C_{D_0}}\right] \qquad (38)$$

$$f_2' = \frac{hs}{D_0^2}\left[2\zeta\omega + \frac{2\dot{D}_0}{D_0} - \frac{3D_0}{V_0}\right] \qquad (39)$$

$$f_3' = \frac{hs}{D_0^3}\left[\frac{3\dot{D}_0D_0}{V_0^2} + \frac{8D_0^3}{V_0^3} - \frac{2D_0V_0}{hsr_0} - \frac{\dot{C}_{D_0}D_0^2}{C_{D_0}V_0^2}\right] \qquad (40)$$

To avoid the difficulty of numerical differentiation for obtaining $\delta\dot{D}$, this feedback term is eliminated by relating δD to δh, which is determined by onboard navigation without the need for numerical differentiation. This transformation is accomplished by applying first-order difference equations to Eq. (25).

$$\delta\dot{D} = -\left(\frac{\dot{h}_0}{hs} + \frac{4D_0}{V_0} - \frac{\dot{C}_{D_0}}{C_{D_0}}\right)\delta D - \frac{D_0}{hs}\,\delta\dot{h} + \frac{2D_0^2}{V_0^2}\,\delta V \tag{41}$$

The control law then becomes

$$\delta(L/D) = f_1\delta D + f_2\delta\dot{h} + f_3\delta V \tag{42}$$

and

$$(L/D)_C = (L/D)_0 + f_1\delta D + f_2\delta\dot{h} + f_3\delta V \tag{43}$$

Then

$$f_1 = f_1' - f_2'\left(\frac{\dot{h}_0}{hs} + \frac{4D_0}{V_0} - \frac{\dot{C}_{D_0}}{C_{D_0}}\right) \tag{44}$$

$$f_2 = -f_2'\frac{D_0}{hs} \tag{45}$$

$$f_3 = f_3' + 2f_2'\frac{D_0^2}{V_0^2} \tag{46}$$

With Earth-relative speed chosen as the independent variable, δV is identically zero. Also, elimination of the $\delta\dot{D}$ feedback term in favor of $\delta\dot{h}$ eliminates the noisy data resulting from numerical differentiation required to obtain $\dot{D}$. However, errors in determining altitude rate, which is unstable using an inertial navigation system, induces a steady state drag acceleration standoff from the reference profile that is proportional to the error in navigated altitude rate. Therefore, a feedback term proportional to the integral of $\delta\dot{D}$ is

introduced to eliminate this steady state error caused by the inaccuracy in determining the Orbiter altitude rate. The resulting control law is as follows:

$$(L/D)_C = (L/D)_0 + f_1 (D - D_0) + f_2 (\dot{h} - \dot{h}_0) + \\ + f_4 \int (D - D_0) \qquad (47)$$

GUIDANCE LOGIC

The guidance concept described in the previous section is a general concept applicable to a wide variety of entry vehicles and planetary environments. Selection of the shape and the number of drag acceleration profile segments is dependent on the vehicle configuration, vehicle constraints, and the type of mission to be flown. For the Space Shuttle Orbiter, five basic drag reference segments were selected. Two quadratic segments are used during the region of aerodynamic heating that occurs at high speeds. A pseudoequilibrium glide segment and a constant drag segment are used in the intermediate speed region. A linear segment, which is a function of energy, is used in the low speed region. The shape of each segment and the segment intersection points are located in the erasable memory of the flight computer. These constants can be changed premission or during the mission. This permits flexibility in optimizing the entry profile based on mission requirements and Orbiter capability. Figures 3 (a) and (b) present the drag reference

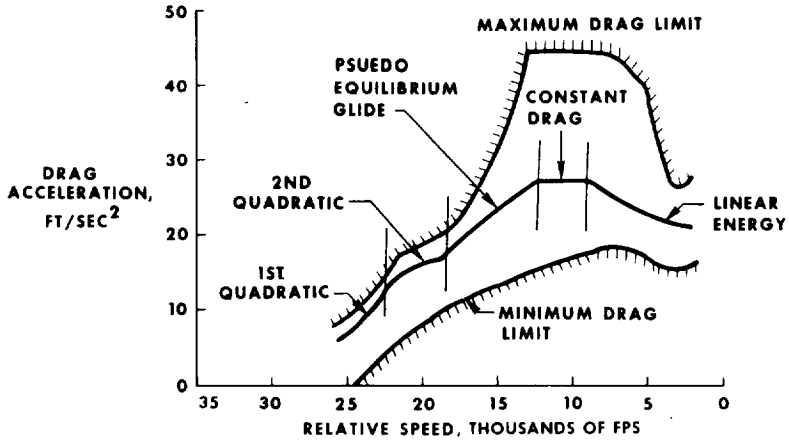

(a) Operational angle-of-attack profile.

Figure 3.- Reference drag profile.

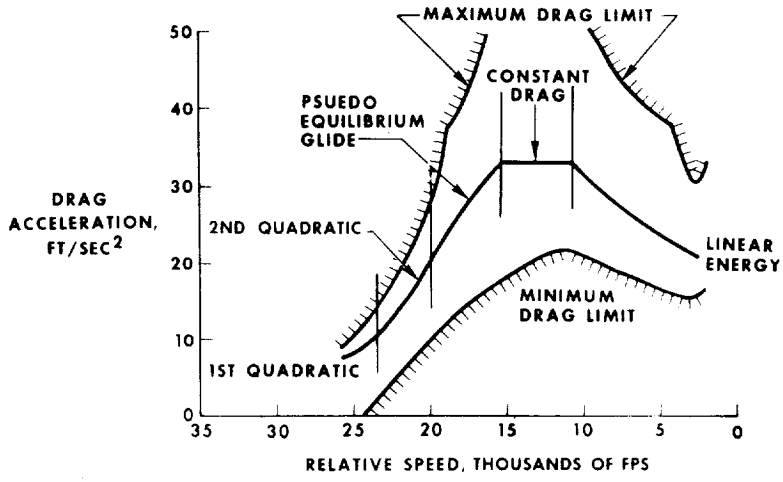

(b) Flight test program angle-of-attack profile.

Figure 3.- Concluded.

profile shapes for the 38/28 degree profile, typical of operational flights and the 40-degree angle-of-attack profile to be used in the early flight test program. By use of the shaping constants, the five-drag profile segments can be selected optimally for both angle-of-attack situations.

Ranging Method and Range Equations

Once the shape of the drag profile is selected, range errors are nulled by adjusting the magnitude of the drag reference profile while retaining the fundamental profile shape. Several options can be used in adjusting the reference drag profile for nulling range errors. The total profile may be adjusted to change the range potential, or only part of the profile may be adjusted. For the Orbiter, the technique for adjusting the reference drag profile for ranging depends on the guidance phase being executed.

It is necessary to preserve the postblackout footprint capability as long as possible because the Orbiter must be able to accommodate significant navigation errors and make corrections for these errors after the exit from communications blackout, at approximately 150 000 ft altitude.

Further, the postblackout footprint capability must be preserved because the Orbiter must also have the capability to change landing directions on the runway to accommodate landing wind changes that may occur after the last ground communications before deorbit. Therefore, the reference drag segments are connected, and the reference profile adjustments for ranging are designed to preserve the postblackout ranging capability. The first guidance phase is the temperature control phase that consists of two quadratic drag segments, which are functions of Earth-relative speed. This phase is followed by the equilibrium glide phase, the constant drag phase, and finally by a linear drag-energy phase called the transition phase. During the temperature control phase, the Orbiter range errors are nulled by adjusting the temperature control quadratics and the equilibrium glide profile as illustrated in Fig. 4 (a) by means of analytic paritial derivatives of range with respect to the drag profile changes. During the first two guidance phases, the constant drag level and the range flown during the transition phase is not altered. The effect of this arrangement is to drive the trajectory back to nominal at the start of the constant drag phase.

In a similar manner during the equilibrium glide phase, range errors are nulled by adjusting the level of the equilibrium glide drag profile with both the constant drag level and the transition range remaining constant. During the constant drag phase, only the level of the constant drag phase is changed to achieve ranging while the transition phase range is held constant. Only during the transition phase itself, is the transition phase ranging potential used. This ranging process preserves the postblackout ranging capability by maintaining a near nominal state at blackout exit. Figs. 4 (a) through (d) present a summary of the ranging technique, and Table 3 presents the range equations and analytic equations for the partial derivative of range with respect to the drag profile adjustment.

Profile Reference Parameters

Once the desired drag profile is computed, i.e., every 1.92 seconds for

the Orbiter, the reference trajectory parameters D_0, h_0, and $(L/D)_0$ must be computed along with the controller gains f_1, f_2, and f_4.

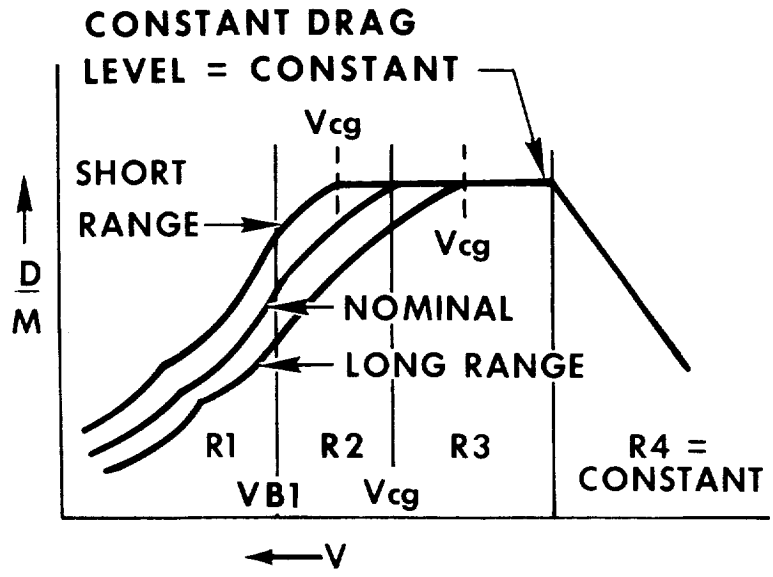

(a) Temperature control phase.

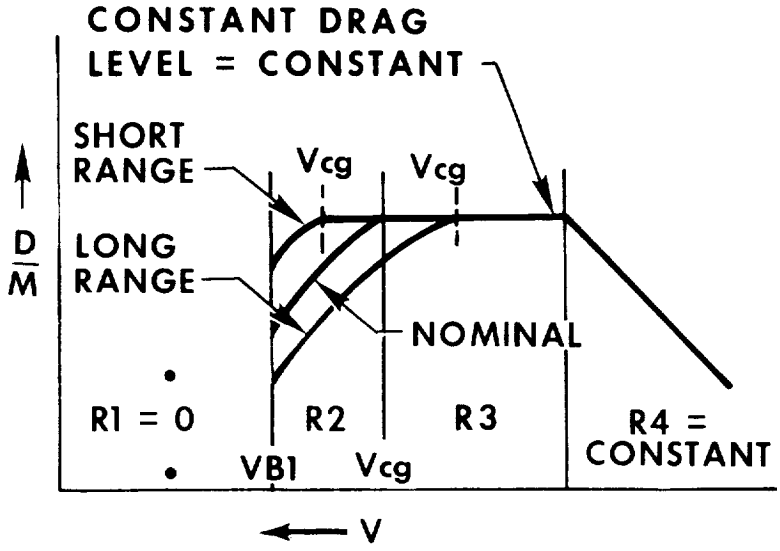

(b) Equilibrium glide phase.

Figure 4.- Ranging technique.

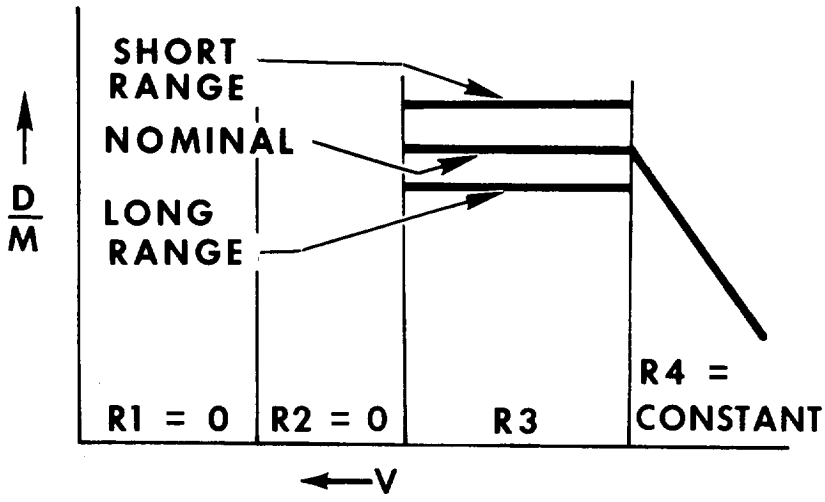

(c) Constant drag phase.

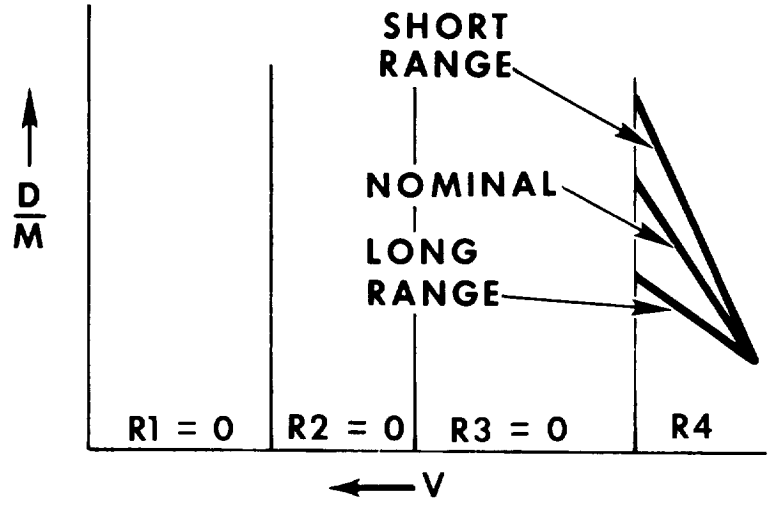

(d) Transition phase.

Figure 4.- Concluded.

The drag reference parameter, D_0, is simply the current desired drag acceleration level from the drag profile that matches the profile range potential and the current range-to-go from the navigation system. The altitude rate reference term $\dot{h}_0$ is computed from the theoretical equation derived earlier (Eq. (25)) and is presented in Table 2. The $\dot{C}_D/C_D$ term is a function of the angle-of-attack reference profile. This term is developed using empirical equations for the Orbiter aerodynamic drag coefficients:

$$C_D = K_1 + K_2\alpha + K_3\alpha^2 + K_4 e^{-\left(\frac{V - K_5}{K_6}\right)} \tag{48}$$

and $\dot{C}_D$ is equal to the time derivative of C_D

$$\dot{C}_D = K_7 (D + g\dot{h}/v) \; e^{-\left(\frac{V - K_5}{K_6}\right)} + \dot{\alpha}_0 (K_8 \alpha_0 + K_9) \tag{49}$$

TABLE 3.- RANGE PREDICTION MECHANIZATION

Phase	Range Equation Constraints	Total Range Prediction	dR/dD
Temperature Control	R4 = Constant C4 = Constant	$R_1 + R_2 + R_3 + R_4$	$-\frac{R_1 + R_2}{(D_0 \text{ at VB1})}$
Equilibrium Glide	R4 = Constant C4 = Constant	$R_2 + R_3 + R_4$	$-\frac{R_2}{(D_0 \text{ at Vcurrent})}$
Constant Drag	R4 = Constant	$R_3 + R_4$	None, R_3 can be solved directly
Transition	None	R_4	$\frac{D_0 - D_F - (C_5 D_0 R_4)}{C_5 D_0 (D_0 - D_F)}$

The coefficients K_1 - K_9 are dependent on the vehicle aerodynamic drag coefficient characteristics. The constants K_7 - K_9 provide additional flexibility in curve fitting C_D and $\dot{C}_D$.

The reference L/D ratio, $(L/D)_0$, is computed from Eq. (32). However, some of the terms in Eq. (32) are negligible and can be deleted to save computer core and execution time. Table 4 presents the reference L/D equation for each of the guidance phases with the negligible terms deleted. In general, the $\dot{C}_D$ terms in the L/D reference equation were deleted in all of the guidance phases.

Control Law Gains

Eqs. (44) and (45) presented the theoretical gains for the control law,

TABLE 4.- SIMPLIFIED $(L/D)_0$ EQUATIONS

Phase	Simplified Equation
Temperature Control	$\frac{g}{D_0}\left(1 - \frac{V^2}{V_S^2}\right) - \frac{4hsC_1}{V^2} - \frac{hsC^2}{V}$
Equilibrium Glide	$\frac{g}{D_0}\left(1 - \frac{V^2}{V_S^2}\right) - \frac{4hsD_0}{V^2\left(1 - \frac{V^2}{V_S^2}\right)}$
Constant Drag	$\frac{g}{D_0}\left(1 - \frac{V^2}{V_S^2}\right) - \frac{4hsD_0}{V^2}$
Transition Phase	$\frac{g}{D_0}\left(1 - \frac{V^2}{V_S^2}\right) + \frac{2V\dot{h}_0 + 2\dot{h}_0 \frac{g}{D} + 2D_0hs + 2g\dot{h}\frac{hs}{V}}{V^2 + 2ghs} + \frac{\dot{h}_0}{V} + \frac{g\dot{h}_0^2}{DV^2}$

which is Eq. (47). Because these equations are complex and very lengthy, an empirical curve fit as a function of drag acceleration is used in the flight software. The period used for the theoretical gains was varied depending on the drag acceleration level. The period varied from approximately 200 sec at low drag levels to 90 sec at high drag levels. Fig. 5 presents the resultant control gains using the following empirical equations

$$f_1 = f_5 D^{f6} + f_9 (D - D_0) \tag{50}$$

$$f_2 = f_7 D^{f8} \tag{51}$$

where f5, f6, f7, f8, and f9 are empirically derived constants used to fit the f1 and f2 theoretical functions. The last term in Eq. (50) is included to improve the phugoid damping characteristics following bank reversals used for crossrange trajectory control.

Flight Control Command Equation

The L/D command equation (Eq. (47)) is used by the guidance to null range errors while maintaining good trajectory and Orbiter attitude transient response characteristics by maintaining the actual drag level near

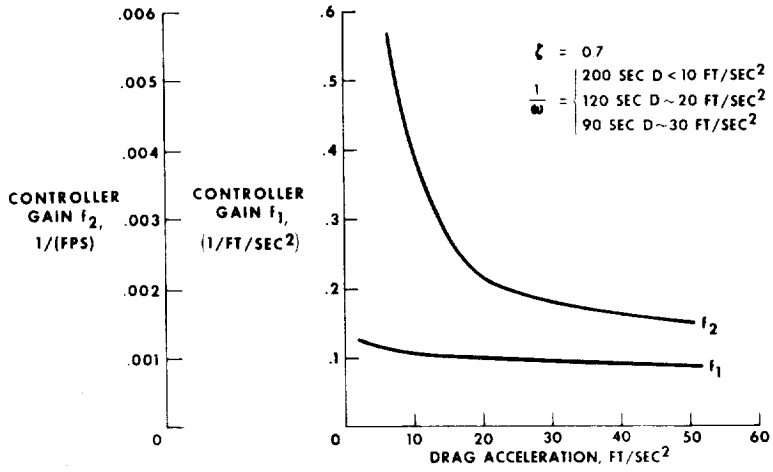

Figure 5.- Controller gains f1 and f2.

the drag reference profile. The L/D command, $(L/D)_C$, can be converted into either a bank angle command or an angle-of-attack command, or a combination of the two. For the Orbiter, both bank angle and angle-of-attack modulation is used for trajectory control. Bank angle modulation is the primary control variable and is computed as follows:

$$\phi_c = \cos^{-1}\left[\frac{(L/D)_c}{L/D}\right] + f_{11}\,(\alpha - \alpha_0) \tag{52}$$

where L/D is the inflight estimated Orbiter L/D derived from stable platform acceleration data in the navigation system. Fig. 6 presents the drag profile history for a nominal entry profile without the contribution from the last term. As can be seen in this figure, the actual drag level is maintained on the desired drag reference profile except for transient maneuvers induced by a bank reversal required for crossrange control. During a bank reversal, the drag level drops below the desired level as the bank angle is rolled through zero with the resultant temporary increase in the inplane component of lift. After the bank reversal, the trajectory must be restabilized on the desired profile. To minimize the effect of the bank reversals and the resultant phugoid motion and other transient effects such as density gradients, a change in angle of attack from the nominal profile is commanded to compensate for short-period drag profile deviations from the reference profile, which

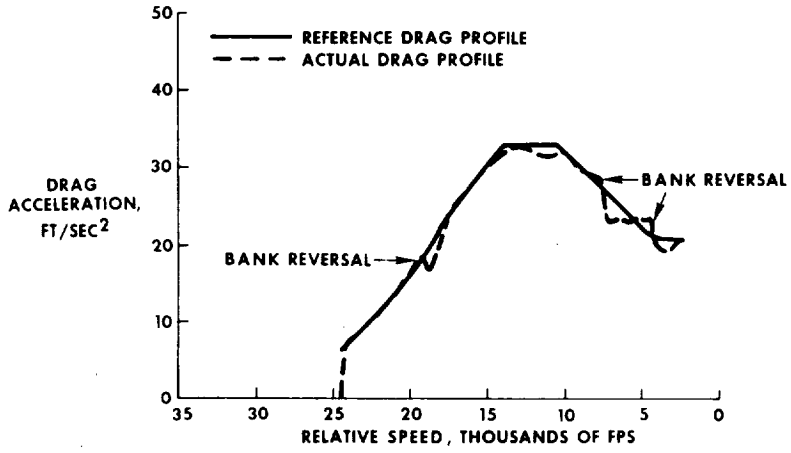

Figure 6.- Drag profile for bank modulation only.

bank angle modulation cannot control. Short period drag control is accomplished by angle-of-attack modulation at a much faster rate by changing the drag coefficient than by bank modulation. This changes the flightpath and thus achieves drag modulation capability through a long period change in atmospheric density. This change in angle-of-attack command from the reference angle-of-attack profile is computed by the equation

$$\Delta\alpha = C_D(D_0 - D)/f_{10} \tag{53}$$

However, because it is desirable to maintain a fixed angle-of-attack-profile, the last term in Eq. (52) is included to drive the modulated angle of attack back to the reference angle-of-attack schedule, on a long term basis. Fig. 7 presents the resultant drag profile with both bank angle and angle-of-attack modulation for drag control. A comparison of this figure with Fig. 6 shows that angle-of-attack modulation has compensated for the drag transients associated with bank angle modulation only. Fig. 8 presents the angle-of-attack history for this case and shows that the bank bias logic successfully drove the actual angle of attack back to the desired schedule.

Lateral Logic

Crossrange is controlled by a series of bank angle reversals determined by an azimuth error deadband as illustrated in Fig. 9. The azimuth

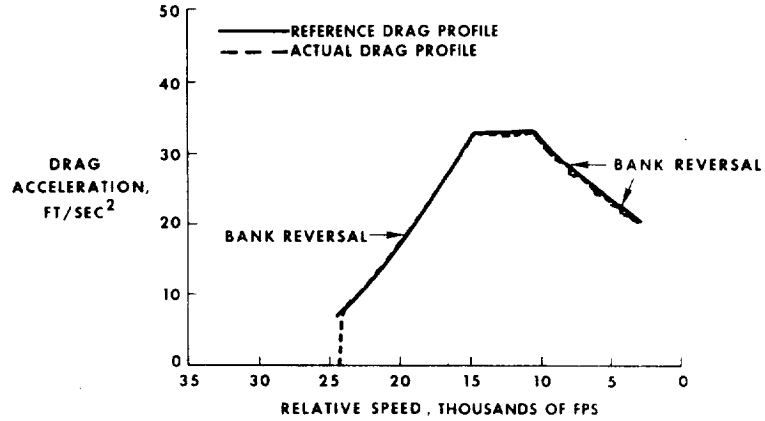

Figure 7.- Drag profile for bank and angle-of-attack modulation.

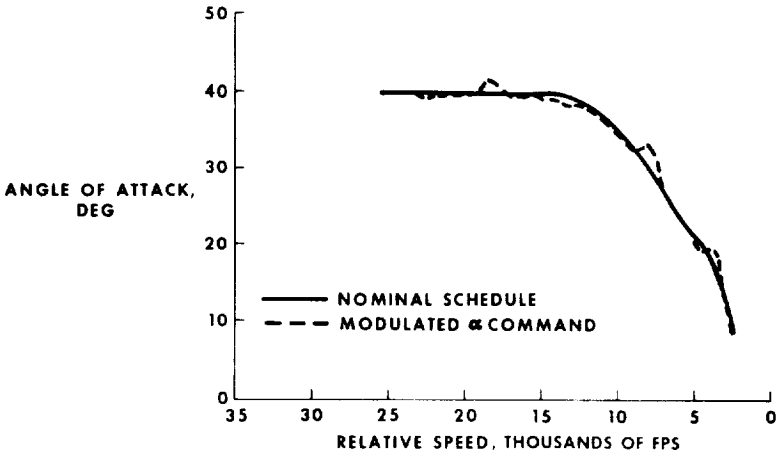

Figure 8.- Angle-of-attack profile for bank and angle-of-attack modulation case.

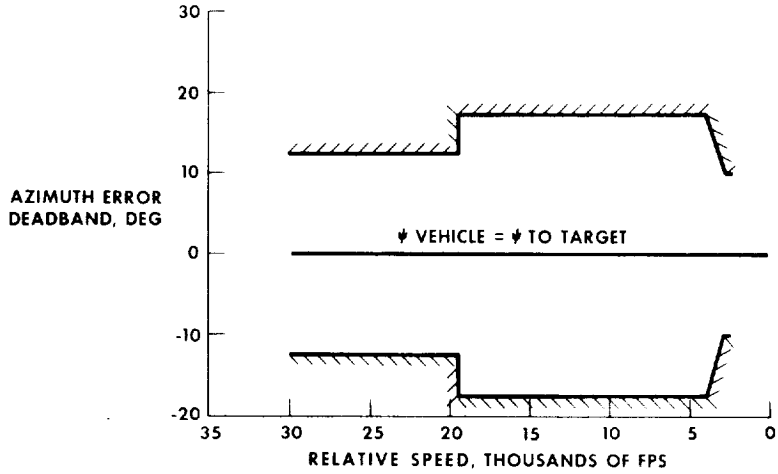

Figure 9.- Azimuth error deadband.

error is the angle between the plane formed by the Orbiter position and velocity vectors and the plane formed by the Orbiter position vector and a vector from the Orbiter to a target point on a heading alignment circle positioned near the runway. This geometry is illustrated in Fig. 10. Because the magnitude of the bank angle is determined by the drag error and altitude rate error requirements in the controller equation, no special computations are made for crossrange control except for the application of a minimum bank angle to maintain crossrange control for cases where inplane ranging considerations result in very small bank angle commands.

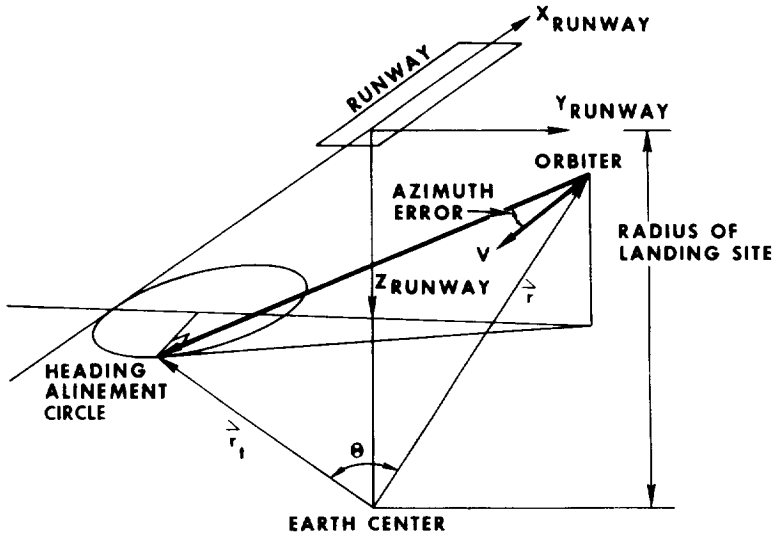

Figure 10.- Entry azimuth error geometry.

PERFORMANCE ANALYSIS

The entry guidance system must perform satisfactorily over a wide range of initial conditions and in the presence of navigation system errors, environmental dispersions, and vehicle aerodynamic uncertainties. The results of a 50-sample Monte Carlo dispersion analysis is presented to demonstrate the performance of the entry guidance system. This dispersion analysis includes models for initial navigation state errors, platform misalignments, accelerometer errors, gyro drifts, aerodynamic lift and drag coefficient errors, atmospheric density-pressure-temperature errors, atmospheric winds, and external ground navigation system errors.

These error sources were randomly selected, and the result of the 50-case Monte Carlo analysis are presented in Figs. 11 through 15.

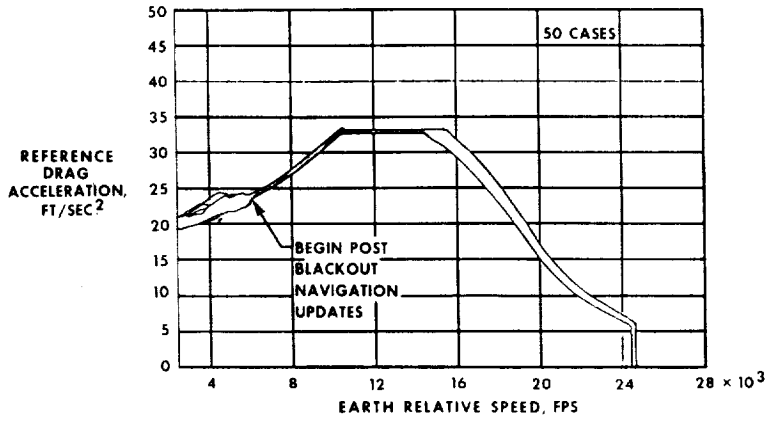

(a) Drag reference profile.

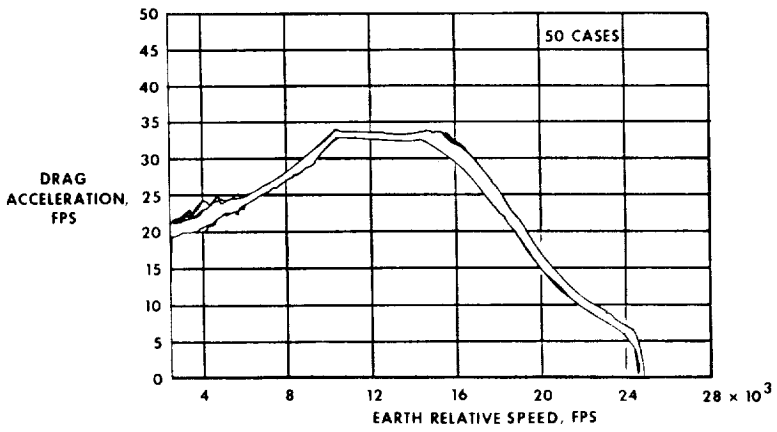

(b) Actual drag profile.

Figure 11.- Drag acceleration profiles.

Fig. 11 (a) presents a composite plot of the drag reference profiles for each of the 50 Monte Carlo cases and Fig. 11 (b) presents the actual drag acceleration profiles for the same cases. A comparison of these two figures illustrates that the guidance controller equation sucessfully controlled drag to the drag reference throughout the entry. Figs. 12 and 13 show the bank angle and angle-of-attack profiles required for trajectory control. Figs. 14 and 15 show the composite

plots of the normal load factor and dynamic pressure profiles for the 50 Monte Carlo cases. As can be seen from these figures, the guidance did

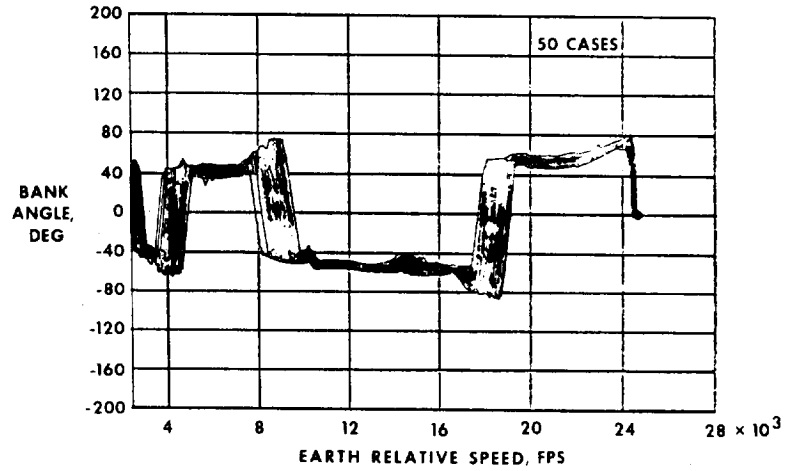

Figure 12.- Bank angle profile from Monte Carlo analysis.

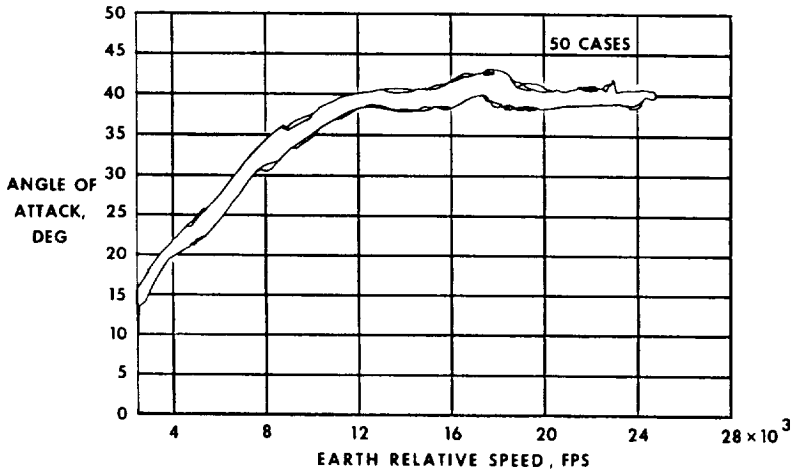

Figure 13.- Angle-of-attack profiles from Monte Carlo analysis.

not cause the trajectory to approach Orbiter limits. At a relative speed of 2500 fps, the entry guidance terminated with a 3σ range error of ± 2.2 nmi as compared to the ± 5 nmi accuracy requirement. These data illustrate that the analytic drag control entry guidance developed for

the Orbiter is not only a viable concept but more than adequately meets all Orbiter entry constraints and objectives.

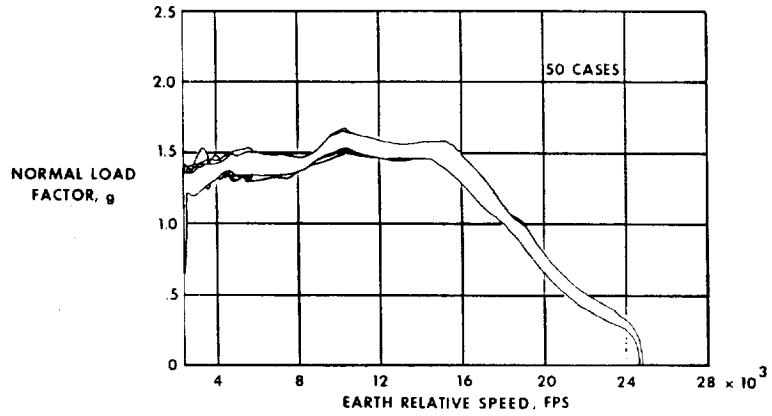

Figure 14.- Normal load factor profile from Monte Carlo analysis.

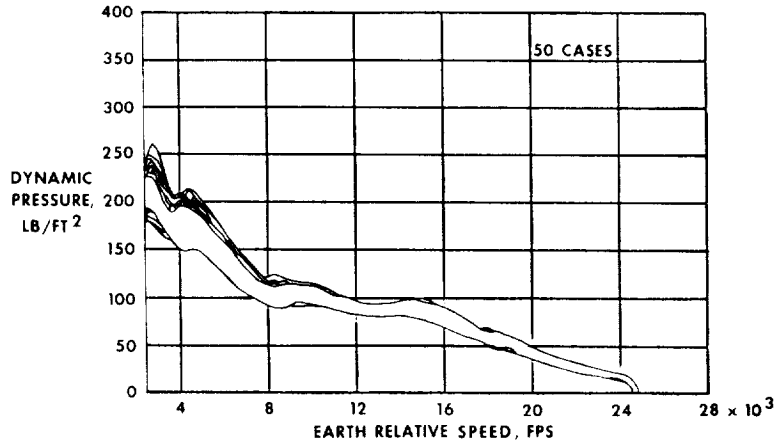

Figure 15.- Dynamic pressure profiles from Monte Carlo analysis.

CONCLUSION

The Shuttle entry guidance meets the design objectives of providing the flexibility to accomodate a wide variety of missions within the Orbiter systems and operational constraints. This guidance is based on a control law that ensures damping of oscillatory type trajectory motion to control the Orbiter to an analytically computed drag acceleration profile. This drag acceleration profile is defined by a set of erasable memory constraints that can be changed to adapt to different mission and

system requirements. Both the range prediction equations and the computation of the reference trajectory parameters are analytically computed each computer cycle during entry.

Although this guidance concept was developed for the Space Shuttle Orbiter, it is applicable for any entry vehicle with aerodynamic lift that can be modulated for trajectory control. The only requirement for different applications is that the shape and number of drag profile segments be selected for the individual vehicle constraints and mission requirements.

SYMBOLS

C_1 = arbitrary constant
C_2 = arbitrary constant
C_3 = arbitrary constant
D = drag force per-unit-mass
E = energy per-unit-mass
f_1' = function for control law feedback gains
f_2' = function for control law feedback gains
f_3' = function for control law feedback gains
f_1 = function for control law feedback gains
f_2 = function for control law feedback gains
f_3 = function for control law feedback gains
f_4 = function for control law feedback gains
f_5 = function for control law feedback gains
f_6 = function for control law feedback gains
f_7 = function for control law feedback gains
f_8 = function for control law feedback gains
f_9 = function for control law feedback gains
f_{10} = gain in $\Delta\alpha$ equation
f_{11} = gain in roll bias equation
g = gravitational acceleration
h = altitude above the Earth's surface
$\dot{h}$ = altitude rate above the Earth's surface

hs = atmospheric density scale height

K_1 = constant in C_D curve fit

K_2 = constant in C_D curve fit

K_3 = constant in C_D curve fit

K_4 = constant in C_D curve fit

K_5 = constant in C_D curve fit

K_6 = constant in C_D curve fit

K_7 = constant in C_D curve fit

K_8 = constant in C_D curve fit

K_9 = constant in C_D curve fit

L/D = ratio of the lift force component in the Earth-relative velocity-radius vector plane to the drag force

L_V = lift force per-unit-mass

R = range

r = distance from the center of the Earth to the Orbiter

V = Earth-relative speed

VB1 = junction point between temperature control phase and equilibrium glide phase

V_F = end speed for each guidance phase

V_S = arbitrary constant in equilibrium glide equation

α = angle of attack

γ = angle between the local horizontal plane and the Earth-relative velocity vector

δ = () small increment in ()

ζ = damping ratio

θ = geocentric latitude

ρ = atmospheric density

ρ_0 = atmospheric density at base altitude

ϕ = bank angle

ψ = azimuth of Earth-relative velocity vector

ω = undamped natural frequency

. = time derivative (superscript)

c = command (subscript)

0 = value on reference trajectory (subscript)